Electrorotation Measurements of Diamide-Induced Platelet Activation Changes

Marcel Egger* and Edwin Donath‡
*Physiologisches Institut der Universität Zürich, CH-8057 Zürich, Switzerland, and ‡Biologisches Institut, Humboldt-Universität zu Berlin, 10115 Berlin, Germany

ABSTRACT Electrorotation is a special dielectric spectroscopic technique capable of measuring the polarizability of single platelets. The rotational speed of the particles is recorded as a function of the frequency of the applied rotating electric field. As previously shown, the speed of electrorotation in the range of the first characteristic frequency (anti-field rotation) decreased upon activation and was correlated with [^{14}C]serotonin release and an increase of the TMA-DPH-induced fluorescence. Diamide incubation induced morphological changes in control platelets. These changes were accompanied by a shift of the first characteristic frequency of electrorotation toward higher values and a parallel increase of the anti-field rotation. This was explained by a decrease of membrane conductivity and by the changed polarizability of platelet interior due to the observed internal platelet structure changes. Diamide inhibited activation assessed by both electrorotation and TMA-DPH fluorescence in the case of all activators except the ionophore A 23187. Because diamide largely inhibited the A 23187-induced serotonin release, it was concluded that, despite the diamide treatment, the direct increase of cytoplasmic Ca^{2+} was still able to induce membrane conductivity changes accessible by electrorotation, but this did not complete the final release step of the activation process.

INTRODUCTION

Electrorotation is a dielectric spectroscopic technique for measuring the polarizability of biological or nonbiological particles (Fuhr and Kuzmin, 1986; Kakutani et al., 1993; Pastushenko et al., 1985, 1988; Sauer and Schlögel, 1985; Wang et al., 1993). Particle rotation is induced by the application of a rotating electric field, and the intensity and direction of particle rotation are recorded as a function of the external electric field frequency. In the case where the structure of the particle is known and is sufficiently simple, the dielectric parameters of the particle can be assessed. In recent years electrorotation has been successfully applied to studying the dielectric properties of various particles and cells (Arnold and Zimmermann, 1988; Asami and Yamaguchi, 1992; Donath et al., 1990; Fuhr et al. 1990; Egger et al., 1991a, b; Gimsa et al., 1991a, b; Gimsa et al., 1993). In a previous study we have shown that electrorotation is a suitable method to assess platelet activation at a single cell level (Egger et al., 1988).

Upon activation, the rotation decreased and ceased completely with strong activators. It was concluded that primarily membrane conductivity changes were responsible for the altered electrorotation behavior upon activation. However, it was not clear at which particular step of the activation process this putative membrane conductivity change occurred. It has been previously shown that hyperosmolar solution inhibited the rotation decrease together with activation. The same result was found with a number of amphipaths. The electrorotation decrease correlated with the [^{14}C]serotonin release at release percentages above 60%. But it did not not correlate with the aggregation potency. Diamide is known to influence the platelet aggregation behavior and to induce metabolic and structural changes as well (Wu et al., 1992; Hill et al., 1989; Spangenberg et al., 1987). Diamide oxidizes protein SH-groups. It disturbs the function of cytoskeleton proteins by affecting disulfide-bridges and changes the sulfhydryl-disulfide status, which is controlled by glutathione. This is decisively important for the platelet functional behavior (Hill et al., 1989). Changes in the diamide-induced platelet morphology and metabolism were accompanied by changes in the platelet aggregation and release behavior (Hoffmann et al., 1983). With red cells and other cell types, changes of the viscoelastic properties of the membrane induced by cross-linking of membrane proteins and also membrane permeability changes were observed (Kitajima et al., 1990; Klonk and Deuticke, 1992).

The object of this present study was to investigate whether the electrorotation change was induced primarily by membrane conductivity changes or whether it depended also on the more complex interplay between metabolic and cytoskeleton-involved processes. The diamide treatment is one way to induce complex changes both in the interactions of cellular pathways and structure by significantly inhibiting protein dependent processes. Here we show that it is possible to correlate morphological changes and changes in the dielectric properties of the platelet membrane with dielectric spectroscopy measurements of electrorotation in low and high frequency ranges.

MATERIALS AND METHODS

Blood collection procedure and serotonin loading

Blood was withdrawn by venous puncture from healthy donors who had taken no drugs during the previous two weeks. Immediately after the venous puncture, the blood was mixed with 1/10 vol of 3.12% (w/v) sodium citrate (pH 7.4). Platelet-rich plasma was prepared by centrifugation at 200 × g for

Received for publication 19 April 1994 and in final form 19 October 1994.
Address reprint requests to M. Egger, Physiologisches Institut, Universität Zürich, Winterthurerstr. 190, CH-8057 Zürich, Switzerland.

0006-3495/95/01/364/09 $2.00

15 min at room temperature. The supernatant platelet-rich plasma was incubated with 1.0 μM 5-hydroxy(side-chain-2-[^{14}C]tryptamine)creatinine ([^{14}C]-serotonin, sp. radioactivity 55 mCi/mmol, CFA 170, The Radiochemical Centre, Amersham, U.K.) for 30 min at 37°C. Measurement of serotonin release was performed according to Heptinstall et al. (1980). After centrifugation of platelet-rich plasma, 300 × g, 15 min, room temperature, the platelets were washed 2 times with a procedure described earlier (Egger et al., 1988). The platelets were resuspended in HEPES-Tyrode buffer (5.55 mM glucose, 5.45 mM NaH_2PO_4, 0.01 mM $MgCl_2$) adjusted to pH 7.35.

Diamide-modified platelets

The washed platelets were incubated with 0.5 mM diamide (azodicarboxylic-acid-bis-dimethylamide, Sigma Chemical Co., St. Louis, MO) for 5–60 min at 37°C in HEPES-Tyrode buffer.

Platelet activation

The platelet activation was induced with the same activator concentration at 37°C in fluorescence, electrorotation, aggregation, and secretion measurements. To compare different inducers with regard to their potential for inducing serotonin release, we calibrated the platelet suspension on equal biphasic, irreversible aggregation traces for each blood sample as described previously (Egger et al., 1988). Platelet activation at 37°C was induced by adding 1.0–4.0 μg/ml collagen (Sigma) 0.1–1.0 units/ml thrombin (Sigma), 1.0–2.5 mM arachidonic acid, or 0.1–0.5 μM A 23187 (Calbiochem, La Jolla, CA).

Fluorescence measurements

The platelet suspension was adjusted to a concentration of 2.5 × 10^8 platelets/ml. The platelet concentration was checked by Coulter counter measurements (Technicon H4, Coulter Counter S plus 4, Coulter Inc. USA). Fluorescence was measured by means of Perkin-Elmer MPF 44 B (Perkin-Elmer Inc., U.K.) trimethylammonium-diphenylhexatriene. TMA-DPH, (Molecular Probes, Eugene, OR) stock solution of 0.5 mM in dimethylformamide was made. Under continuous stirring, TMA-DPH was added into a 4.0 ml quartz fluorescence cuvette containing 3.0 ml of HEPES-Tyrode buffer to yield a final concentration of 1.2 μM. The cuvette was preincubated for 5 min at 37°C. The preliminary measurement of background fluorescence followed. An aliquot of the platelet suspension was added to give a final concentration of 10^7 platelets/ml. The sample was allowed to stand for 4 min, although the incorporation was almost immediate, as was shown by the stabilization of the TMA-DPH fluorescence intensity signal. Excitation and emission wavelengths were 350 and 430 nm, respectively (Bronner et al., 1986a, b). These settings yielded maximal emission. Fluorescence intensity was then continuously recorded both before and during platelet activation. Platelets were stimulated in the cuvette after the initial fluorescence level was recorded for 2 min.

Electrorotation

The platelets were resuspended into the measuring solution: 300 mOsm sucrose, 5.8 mM PBS buffered at pH 7.2. The final cell density was 50–200 platelets/μl. The suspension conductivity was 12 ± 2 mS/m. It was determined before and after rotation measurements with a conductometer LM 301 (Hydromat, Germany) at 22°C. This suspension was kept at 37°C while the measuring chamber and the microscope were adjusted. This lasted no longer than 5 min. The electrorotation chamber consisted of four electrodes (Egger et al., 1988) with an electrode separation of 1.45 mm. The chamber was manipulated with a micromanipulator in a fixed petri dish placed under an inverted microscope. Approximately 200 μl of cell suspension was transferred into the center of the measuring chamber. The measurement immediately followed the platelet sedimentation on the HSA-covered glass surface of the chamber bottom. This was completed within a few minutes. Measurements of electrorotation were performed in a rotating field of 8.0 kV/m, which was generated by square-topped pulses with a duty cycle of 1:1. Either the electrorotation of each individual platelet was measured at selected frequencies in the range of 13 kHz to 30 MHz starting from the MHz range, or the compensation method (Arnold and Zimmermann 1983; Gimsa et al., 1986) was used to determine f_{c1}. The latter uses two electric fields differing both in frequency and in the rotation direction applied in subsequent short intervals. These two fields compensate each other if the applied frequencies are symmetric on the logarithmic scale with respect to the peak frequency. The first characteristic frequencies obtained by fitting of the frequency dependence did not differ from the values measured with the compensation method. In the second characteristic freuency range (f_{c2}) the compensation method could not be used because f_{c2} was close to the upper limiting frequency of the equipment.

Aggregation measurements

In each experiment, platelet aggregation was measured to test the platelet functional performance and to calibrate the platelet samples on equal aggregation traces. The aggregation traces were monitored with a dual channel aggregometer Elvi 80 (Elvi Logos, Italy).

Electron microscopy

For transmission electron micrographs, platelets were fixed for 30 min in glutaraldehyde (2.5%) at room temperature, embedded with Epon, and 50 nm sections were made with Ultrotom 5 (LKB Producta AB, Bromma, Sweden). The sections were viewed in an TEM microscope (Elmiskop 102, Siemens, Germany) at 80 kV voltage.

RESULTS

Control resting platelets were compared with diamide-treated platelets using transmission electron microscopy (Fig. 1, *A* and *B*). As Fig. 1 *B* shows, diamide induced remarkable morphological changes both in the shape and the subcellular organelle distribution and size. After 60 min of diamide treatment, there was an increase of the number of vacuoles and of large granule-free areas. The inner platelet morphology was dramatically changed as a function of the diamide incubation time. The discoid shape of nontreated platelets (Fig. 1 *A*) was transformed into a more irregular one (Fig. 1 *B*). The diamide-induced granule centralization and redistribution resulted in the electron microscopic picture in the formation of noticeable electron-dense zones. The canalicular system provides electric current pathways into and through the particle, thus forming a complex electrical equivalent network within the platelet. Moreover, upon activation the canalicular system widens and changes.

The rotation behavior of diamide-treated platelets was investigated in the first and second characteristic frequency range. Fig. 2 *A* shows that the anti-field peak rotation increased with the diamide incubation time and that the first characteristic frequency was shifted to higher frequencies. After 30 min of diamide treatment, the first characteristic frequency was increased by a factor of two or more. Concomitantly, we observed a large increase of the anti-field peak rotation of about 100%. If the diamide treatment lasted longer than 30 min, the anti-field rotation increased further but the first characteristic frequency was now shifted back to lower values. Fig. 2 *B* demonstrates the diamide influence in the MHz range of co-field rotation. There was a significant

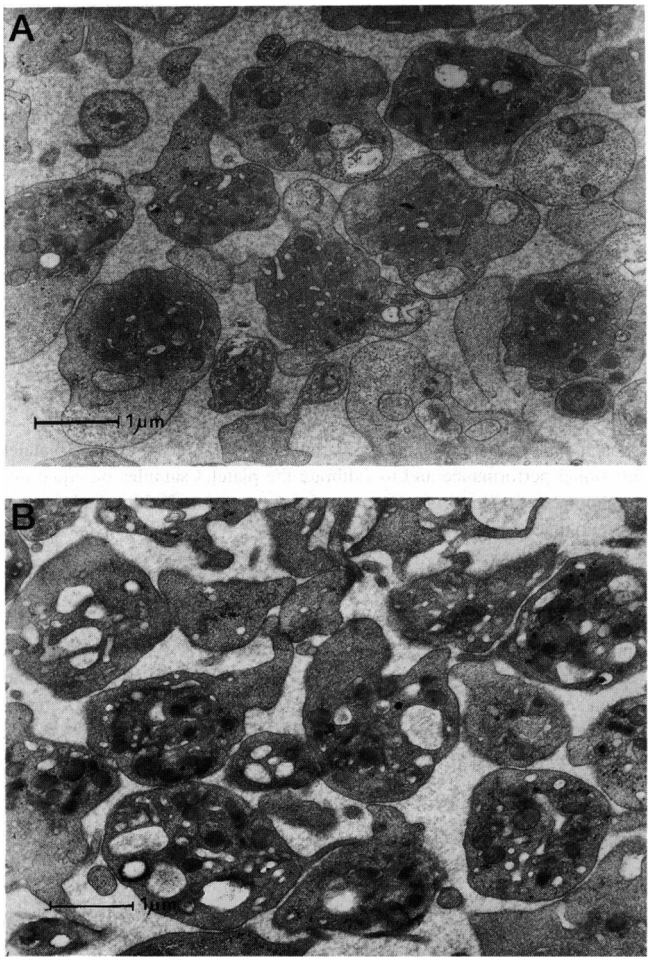

FIGURE 1 Transmission electron micrograph of platelets (×20000) control cells (*A*) and treated with 0.5 mM diamide for 60 min at 37°C (*B*).

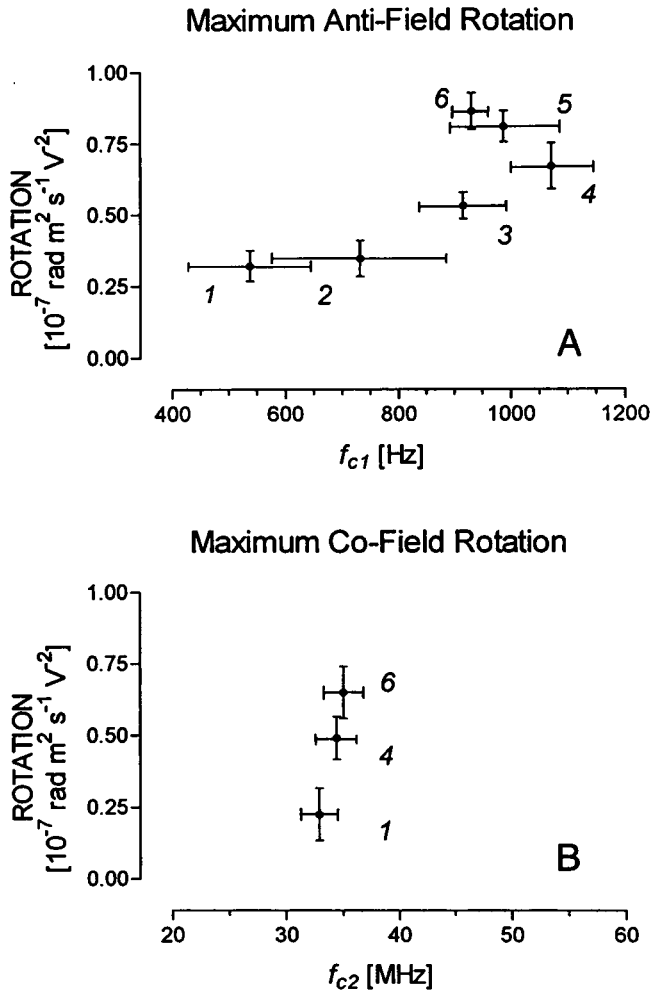

FIGURE 2 Maximum anti-field (*A*) and maximum co-field rotation (*B*) of diamide-treated platelets plotted against the first and second characteristic frequency (f_{c1},f_{c2}). HEPES-Tyrode buffer, 0.5 mM diamide at 37°C; (*A*) (1) control, (2) 5 min, (3) 15 min, (4) 30 min, (5) 45 min, (6) 60 min, (*B*) (1) control, (4) 30 min, (6) 60 min. Measuring solution: 300 mOsm succrose, 5.8 mM PBS, pH 7.2, room temperature, SE, n = 12.

increase of the co-field rotation with increasing diamide incubation time. But in contrast to the anti-field rotation range, no detectable shift of the second characteristic frequency was observed. Measurements after 30 and 60 min of diamide treatment are provided.

It was of interest to investigate whether by means of electrorotation other aspects of activation of diamide-treated platelets could be detected in addition to its largely reduced aggregation, release potency, and surface area increase. Table 1 shows the results of aggregation and [^{14}C]serotonin release measurements. Diamide-treated platelets were activated with a variety of activators. Data with thrombin (0.5 units/ml), arachidonic acid (1.0 mM), and ionophore A 23187 (0.1 μM) are provided. Already, 5 min of diamide-treatment was sufficient to completely inhibit irreversible aggregation. These and other activators were capable of inducing only a transient reversible aggregation. The [^{14}C]serotonin release reaction was only slightly decreased. After 30 and 60 min, neither irreversible nor reversible aggregation was observed. The [^{14}C]serotonin release decreased by about 80% (Table 1).

The change of the anti-field rotation of diamide-treated platelets with and without activation is given in Table 2. Thrombin and arachidonic acid as well as other natural activators were unable to induce a decrease of the anti-field rotation of diamide-treated platelets. However, A 23187 still induced a significant decrease of the anti-field rotation. With increasing time of diamide incubation, there was a small decrease of the efficiency of the rotation decrease induced by ionophore A 23187. The efficiency decreased from about 50% at 5 min to 35% at 60 min of diamide incubation time.

Fig. 3 shows the increase of the TMA-DPH fluorescence upon activation for control and diamide-treated platelets. In control, the fluorescence signal increased rapidly when TMA-DPH was added. TMA-DPH is a marker of the external exposed membrane surface accessible from the bulk solution. Upon platelet activation, the exocytotic reaction causes the exposure of surplus membrane material and the fluorescence concomitantly increases. An increase in the fluorescence intensity of one relative unit corresponded to a 100% increase in the platelet membrane accessible from the incubation medium. Curve 3 shows that for the control with

TABLE 1 Maximum irreversible aggregation potency and [^{14}C]serotonin release of diamide-treated (0.5 mM) platelets at 37°C

	Aggregation potency light transmission (%)			[^{14}C]serotonin release (%)		
Activator	Thrombin	Arachidonic acid	A 23187	Thrombin	Arachidonic acid	A23187
Untreated PRP	100	100	100	63.1	39.2	90.0
PRP diamide incubation time (min):						
5	0	0	0	52.2	21.4	60.0
30	0	0	0	9.4	3.1	17.4
60	0	0	0	0	0.8	15.4

TABLE 2 Peak value of anti-field rotation of diamide-treated (0.5 mM) platelets measured 7 min after activator was added

	Rotation [10^{-7} rotation/rad m^2 s^{-1} V^{-2}]			
		Activator		
Diamide incubation time (min)	Without activator	Thrombin	Arachidonic acid	A 23187
0	0.322 ± 0.12	0.10 ± 0.07	0.15 ± 0.1	0.05 ± 0.02
5	0.338 ± 0.09	0.35 ± 0.20	0.346 ± 0.21	0.145 ± 0.096
30	0.63 ± 0.15	0.59 ± 0.12	0.69 ± 0.14	0.45 ± 0.08
60	0.85 ± 0.09	0.83 ± 0.04	0.82 ± 0.11	0.55 ± 0.013

Measuring solution: 300 mOsm sucrose, 5.8 mM PBS, pH 7.2, room temperature, SE, $n = 8$. Inducer concentrations given in Material and Methods.

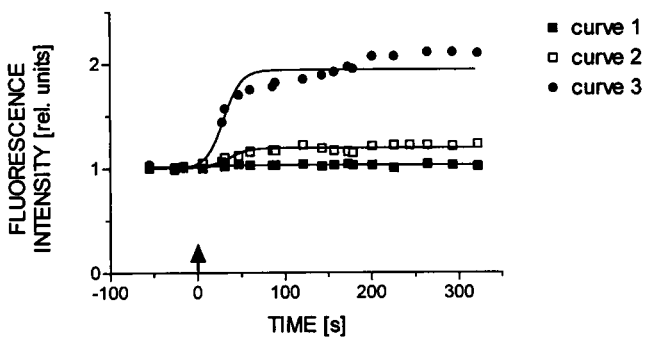

FIGURE 3 Kinetics of TMA-DPH (trimethylammonium-diphenylhexatriene) fluorescence. Curve 1: 0.5 mM diamide treatment for 60 min after thrombin activation. Curve 2: 0.5 mM diamide treatment for 60 min at 37°C and after A 23187, 0.1 μM, activation. Curve 3: A 23187, 0.1 μM, activated platelets without diamide. TMA-DPH concentration in all curves 1.2 mM, 37°C, HEPES-Tyrode buffer.

A 23187 activation the fluorescence intensity increased rapidly, reaching its saturation in less than 300 s. The half-maximum value was approached in about 30 s. Maximum fluorescence intensities of 2.1 rel. units were measured. The release of [^{14}C]-serotonin was equally as fast. Similar fluorescence kinetics induced by thrombin and arachidonic acid were also recorded (not shown). With A 23187, thrombin, and arachidonic acid, the increase of fluorescence intensity correlated with [^{14}C]serotonin release of activated platelets. The [^{14}C]serotonin maximum release rates are given in Table 1 for thrombin, arachidonic acid, and A 23187. After 0.5 mM diamide treatment for 60 min at 37°C, thrombin and arachidonic acid (not shown) were no longer capable of increasing the fluorescence intensity (Fig. 3, curve 1). In contrast, A 23187 was still able to slightly increase the fluorescence intensity as demonstrated in curve 2 of Fig. 3.

DISCUSSION

Electrorotation changes of diamide-treated platelets

The results obtained from the four different methods (platelet aggregation, fluorescence, measurement of [^{14}C]serotonin release, and electrorotation) used here reflect different aspects of the cellular events occurring upon activation. The aggregation method provides information about the physiological reaction of thrombus formation. The exocytotic release was monitored with [^{14}C]serotonin release. The plasma membrane increase accessible from the external solution was detected with TMA-DPH fluorescence, and it is clear that, by means of the electrorotation technique generally, changes in membrane and intracellular conductivities and dielectric structure can be successfully measured. Yet, it was not clear how to quantitatively correlate electrorotation data and the structural changes induced by diamide.

To discuss this question, let us first study the change of electrorotation behavior of nonactivated, diamide-treated platelets in more detail. The most remarkable effect of diamide was that both the anti- and co-field rotation increased gradually with diamide incubation time (Fig. 2, *A* and *B*). The change in the first characteristic frequency was more complex. It was shifted nonmonotonically toward higher frequencies as a function of the diamide incubation time (Fig. 2 *A*). The second characteristic frequency exhibited only a minor shift, if any, upon diamide treatment, as shown in Fig. 2 *B*. This intriguing combination of both the increase of the rotation together with the shift of only the first characteristic frequency to higher values has not been observed with other systems so far investigated by means of electrorotation. Our hypothesis was that the observed complex internal structural changes could be correlated with this behavior.

The electrorotation of single- and multi-shell rotational symmetric particles has been investigated theoretically by Fuhr and Kuzmin (1986) and Sauer and Schlögel (1985). Electrorotation depends on the bulk conductivity, G_e, the membrane conductivity, G_m, the intracellular conductivity, G_i, the radius of the particle, r, the intracellular, membrane, and extracellular dielectric constants, ϵ_i, ϵ_m, and ϵ_e, the

surface conductivity, K_s, and the shell or membrane thickness, h. The torque, N, of a single shell particle shows a characteristic spectrum as a function of the angular frequency, ω, of the applied electric field with field strenght, E, and is given for thin membranes by

$$N = 4\pi\epsilon_0\epsilon_e r^3 E^2 \left[\left(\frac{C_1}{C_2} - \frac{B_1}{B_2} \right) \frac{\omega/\omega_1}{1 + (\omega/\omega_1)^2} + \left(\frac{B_1}{B_2} - \frac{A_1}{A_2} \right) \frac{\omega/\omega_2}{1 + (\omega/\omega_2)^2} \right]. \quad (1)$$

The various coefficients A_1 to C_2 represent combinations of the dielectric parameters and are given by

$$A_1 = \epsilon_m(\epsilon_e - \epsilon_i) + \frac{h}{r}(\epsilon_i - \epsilon_m)(2\epsilon_m + \epsilon_e), \quad (2)$$

$$A_2 = -\epsilon_m(\epsilon_i + 2\epsilon_e) - \frac{2h}{r}(\epsilon_i - \epsilon_m)(\epsilon_e - \epsilon_m), \quad (3)$$

$$B_1 = -G_m(\epsilon_e - \epsilon_i) - \epsilon_m(G_e - G_i) - \frac{h}{r}[(G_i - G_m)(2\epsilon_m + \epsilon_e) + (\epsilon_i - \epsilon_m)(2G_m + G_e)] + \frac{2K_S}{r}\left[\epsilon_m - \frac{h}{r}(\epsilon_m - \epsilon_i) \right], \quad (4)$$

$$B_2 = -G_m(\epsilon_i + 2\epsilon_e) - \epsilon_m(G_i + 2G_e) + \frac{2h}{r}[(G_i - G_m)(\epsilon_e - \epsilon_m) + (\epsilon_i - \epsilon_m)(G_e - G_m)] + \frac{2K_S}{r}\left[\epsilon_m - \frac{h}{r}(\epsilon_m - \epsilon_i) \right], \quad (5)$$

$$C_1 = -G_m(G_e - G_i) - \frac{h}{r}(G_i - G_m)(2G_m + G_e) + \frac{2K_S}{r}\left[G_m - \frac{h}{r}(G_m - G_i) \right], \quad (6)$$

and

$$C_2 = G_m(G_i + 2G_e) + \frac{2h}{r}(G_i - G_m)(G_e - G_m) + \frac{2K_S}{r}\left[G_m - \frac{h}{r}(G_m - G_i) \right]. \quad (7)$$

In Fig. 4 we show the theoretical dependence of the rotation for a single shell particle as a function of the first characteristic frequency, f_{c1}, varying several of the theoretical parameters while keeping the others constant. It was obvious that none of these parameters alone could explain the observed anti-field rotation behavior. Moreover, as demonstrated in Fig. 4 *B*, it was not possible to explain the increase of the magnitude of the second characteristic rotation peak by making changes to any one of the parameters within the framework of the single-shell theory when the internal conductivity was kept within a reasonable range.

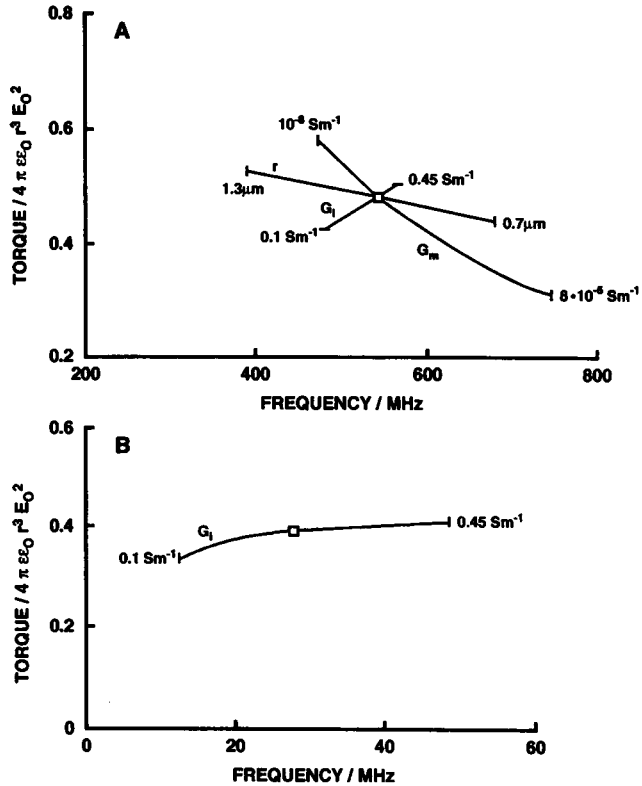

FIGURE 4 Dimensionless maximum torque plotted against the first (*A*) and second (*B*) characteristic frequency of human platelets calculated by means of the single-shell model. (*A*) First characteristic frequency range (□): theoretical control value of the peak anti-field torque and the frequency of the first peak. Bulk solution conductivity: $G_e = 0.012$ S/m, intracellular conductivity: $G_i = 0.25$ S/m, membrane conductivity: $G_m = 1.0 \times 10^{-6}$ S/m, dielectric permittivity of the membrane, $\epsilon_m = 6.0 \times \epsilon_o$, hydrodynamic platelet radius, $r = 0.9$ μm, surface conductivity, $K_s = 10^{-9}\ \Omega^{-1}$, dielectric permittivity of the platelet interior, $\epsilon_i = 50 \times \epsilon_o$, dielectric permittivity of bulk solution, $\epsilon_e = 75 \times \epsilon_o$, membrane thickness, $h = 8.0 \times 10^{-9}$ m. The membrane conductivity (G_m), intracellular conductivity (G_i), and radius (r) were varied each separately. The other parameters were kept constant; (*B*): second characteristic frequency range (□): theoretical control value of the peak co-field torque and the frequency of the second peak; cellular and bulk solution parameters given in *A*. The intracellular conductivity (G_i) was varied separately. The other parameters were kept constant.

We consider that one of the major shortcomings of the available theories is that they only hold for spherically symmetrical particles without internal structure. Neither the polarization of nonspherical geometries nor the contribution of frictional behavior has been systematically studied yet. In the case of platelets we have nonsymmetrical particles with invaginations and with deeply structured intracellular material. Morphological studies with electron microscopy showed that diamide treatment of platelets led to granular centralization in parallel with the formation of large granule-free areas as a function of diamide incubation time (Fig. 1, *A* and *B*). We were convinced that these remarkable morphological changes, both in the shape and the subcellular organelle distribution and size, could not be ignored when interpreting the electrorotation data.

Recently, a closely packed vesicle system surrounded by a common membrane was used to describe theoretically the electrorotation behavior of aggregated particles and

exocytotic cells (Donath et al., 1993). We have suggested a cubically packed cell interior as schematically depicted in Fig. 5. Each internal cubic particle is composed of an interior isotropic phase separated from the exterior by a thin membrane referred to below as a vesicle membrane. Consequently, the whole system comprises two different membrane systems. We have then described the dielectric properties of the interior by averaging the dielectric behavior of the individual elements and have obtained the dielectric constant and the conductivity of the interior now as frequency-dependent parameters.

brane, and "vesicle" interior, respectively, and d is the gap thickness between the "vesicles." For details, the reader is referred to Donath et al. (1993).

To demonstrate the limitations as well as the capabilities of this multiparameter model, we made use of it to discuss the diamide-induced changes of the electrorotation behavior of platelets. In view of the approximate nature of the model and because of the large number of free parameters, it is not meaningful to fit the the experimental data to the theoretical model without explicitly taking account of the observed diamide-induced morphological changes (Fig. 1, *A* and *B*).

$$\epsilon_i = \frac{1}{L+d}\left[C_g + \frac{\left(\frac{C_m}{R_i}+\frac{C_i}{R_m}\right)\left(\frac{2}{R_i}+\frac{1}{R_m}\right)\left(\frac{1}{R_m R_i}-\omega^2 C_m C_i\right)(2C_i+C_m)}{\left(\frac{2}{R_i}+\frac{1}{R_m}\right)^2+\omega^2(2C_i+C_m)^2}\right] \tag{8}$$

$$G_i = \frac{1}{L+d}\left[\frac{1}{R_g} + \frac{\frac{1}{R_m R_i}-\omega^2 C_m C_i\left(\frac{2}{R_i}+\frac{1}{R_m}\right)+\omega^2\left(\frac{C_m}{R_i}+\frac{C_i}{R_m}\right)(2C_i+C_m)}{\left(\frac{2}{R_i}+\frac{1}{R_m}\right)^2+\omega^2(2C_i+C_m)^2}\right] \tag{9}$$

where $C_m = \epsilon_m L/h$, $R_m = h/G_m L^2$, $R_i = 1/G_i L$, $C_i = \epsilon_i L$, $R_g = 1/2d\epsilon_g$, and $C_g = 2d\epsilon_g$. h is the thickness of the "vesicle" membrane. The indices g, m, and i refer to the gap, membrane, and "vesicle" interior, respectively, and d is the gap thickness between the "vesicles." For details, the reader is referred to Donath et al. (1993).

Upon increasing diamide incubation time, the canalicular system widened, thus probably providing a direct electric access from the bulk medium into the platelet interior

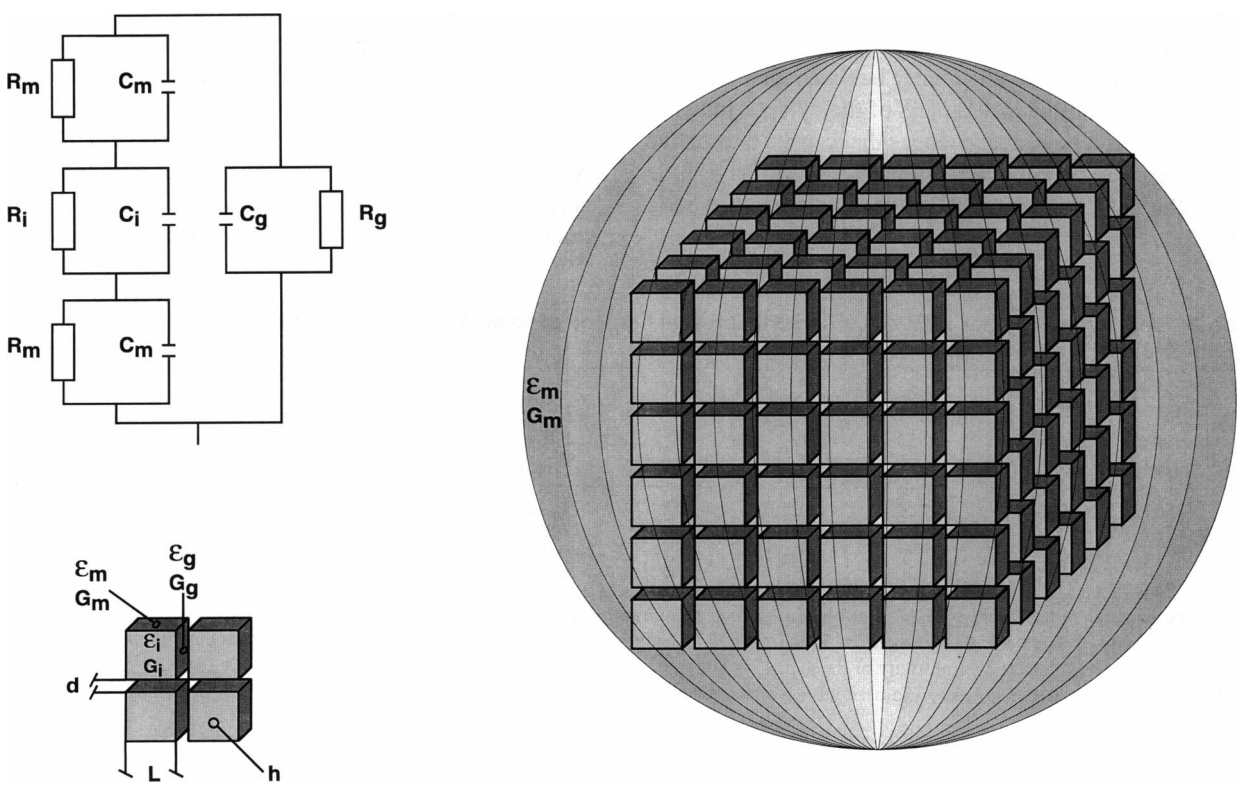

FIGURE 5 Scheme of the cubically structured model and the equivalent circuit. *R* and *C* corresponds to the resistances and capacitances of the membrane, of the cellular and the "vesicle" interior, and of the gap indicated by the indices *m*, *i*, *g*.

through a continuous electrolyte phase surrounding larger areas of vesicular structures separated by the canalicular membrane from the cytoplasm. These changes resulted in an increase of the gap diameter, a decrease of the gap conductivity toward the bulk value, a decrease of the effective plasma membrane conductivity, and an overall change of the platelet size as well as the "vesicle" size.

By closely adhering to these predicted changes in the dielectric properties of the platelets, we calculated the resulting electrorotation spectra together with the frequency dependent internal conductivities and dielectric constants. The parameters are summarized in Table 3. Using the the parameters of row 1 in Table 3, the corresponding electrorotation spectrum (Fig. 6, curve 1) is seen to be close to the rotation behavior obtained from untreated platelets. The presence of the electrically isolating platelet plasma membrane together with the internal canalicular membrane system causes two separated polarization processes in the anti-field rotation range. These two processes result in a broad theoretical anti-field rotation peak with two maxima. It is clear that because of the more complex geometry of the platelet system, one might not be able to observe these *two* peaks separately.

Upon diamide-treatment, the plasma membrane becomes electrically transparent because the canalicular system opens and the conductivity of the gap decreases in parallel. The high conductivity of the plasma membrane shunts the capacitive component, and the associated low frequency peak disappears. This is demonstrated in curve 2 of Fig. 6. Further changes of the geometry of the system, e.g., increasing size, may shift the characteristic frequency of the anti-field rotation peak backwards to lower frequencies (Fig. 6, curve 3).

The electrorotation behavior in the MHz range is mostly a result of the conductivity difference between the bulk electrolyte and electrically isolated parts of the cytoplasm. Consequently, the morphological changes that caused the change of the electrorotation behavior in the kHz range have little effect on the peak frequency of electrorotation in the MHz range.

Although this theoretical illustration consistently described the experimentally observed electrorotation behavior, by no means does this prove that the used structural equivalent model with the respective dielectric parameters is the only possible model to describe the dielectric response of the system. Despite this general limitation, the subsequent semi-quantitative description of the electrorotation of platelets as well as the geometric shortcomings of the model of the interior used, we are convinced that the general idea is basically correct.

Electrorotation and platelet activation

An important finding from our electrorotation investigations with diamide-treated platelets was that the treatment completely inhibited the electrorotation decrease upon activation with the inducers tested. The only exception was A 23187, which was still able to cause an electrorotation decrease. Even 5 min of diamide treatment was sufficient to inhibit the electrorotation decrease, although the diamide effect on the platelets was not yet saturated. Neither the electrorotation decrease nor fluorescence decrease and serotonin release induced by A 23187 was inhibited completely by diamide.

All experiments performed in this study as well as earlier studies have demonstrated that a consistent qualitative correlation of the electrorotation decrease in the range of the first characteristic frequency with the [^{14}C]serotonin release and TMA-DPH fluorescence increase exists. This suggests that the induced platelet electrorotation change was a measure of exocytosis. It also showed that probably in all cases exocytosis in platelets was accompanied by an increase of the effective plasma membrane conductivity as assessed by electrorotation. Consequently, the observed membrane conductivity increase corresponding to a permeabilization or an electrical connection of the canicular system to the cell exterior seems to be a necessary step or a consequence of exocytosis in platelets. It was also remarkable that the kinetics of the electrorotation decrease coincided with an

TABLE 3 Parameters used for calculation of the theoretical first and second characteristic frequencies and the corresponding peak anti- and peak co-field rotations

	d* (μm)	L‡ (μm)	r§ (μm)	G_g¶ (S/m)	G_m‖ (S/m)	f_{c1} (kHz)	Peak anti-field rotation ($N^{**}/4\pi\epsilon\epsilon_o r^3E^2$)	f_{c2} (MHz)	Peak co-field rotation ($N/4\pi\epsilon\epsilon_o r^3E^2$)
1	0.035	1.0	2.5	0.3	10^{-5}	114.3 665.9	0.26 0.24	34.4	0.36
2	0.1	0.5	2.5	0.01	10^{-2}	938	0.33	33.4	0.23
3	0.1	0.7	3.3	0.01	10^{-2}	728	0.41	31.6	0.28

The following parameters were kept constant. *Vesicle parameters:* membrane thickness, h = 5 nm, dielectric permittivity of the membrane, $\epsilon_m = 5.5^*\epsilon_o$, dielectric permittivity of the "vesicle" interior, $\epsilon_i = 50^*\epsilon_o$, "vesicle" membrane conductivity, $G_m = 10^{-9}$ S/m, internal conductivity of the "vesicle," G_i = 0.3 S/m; *Cell parmeters:* dielectric permittivity of the gap, $\epsilon_g = 80^*\epsilon_o$, dielectric permittivity of the outer cell membrane, $\epsilon_m = 5.5^*\epsilon_o$, conductivity of the external solution, G_e = 0.010 S/m, dielectric permittivity of the external solution, $\epsilon_e = 80^*\epsilon_o$, surface conductivity, K_s = O Ω^{-1}.

* "vesicle" diameter.

‡ gap diameter.

§ cell radius.

¶ conductivity of the gap.

‖ outer cell membrane conductivity.

** torque calculated from Eqs. 1–9.

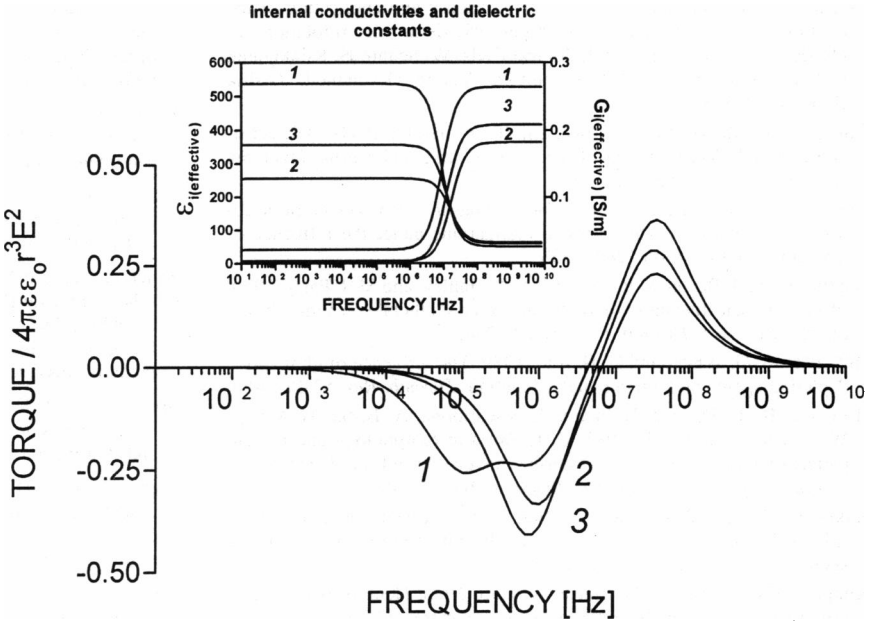

FIGURE 6 Calculated electrorotation spectrum of platelets. The parameters are given in Table 3. The curves corresponds to the number of the rows. (*inset*) Corresponding effective dielectric constant and effective conductivity of the cell interior as a function of the frequency of the electric field.

increase in fluorescence of TMA-DPH. However, there were also quantitative differences of the degree of changes detected by these three methods. Most remarkable was that even after the strongest diamide treatment employed for 60 min, A 23187 still induced an electrorotation decrease of 35%; yet the fluorescence change and serotonin release were much smaller. This was true also for intermediate incubation times. It might be that although the plasma membrane became electrically transparent, at least the exocytotic process, which requires vesicle fusion in addition, was partially inhibited. Probably because diamide-induced inhibition of the functioning of proteins involved in exocytosis did not allow completion of the exocytotic process, i.e., the release of the granule content and the incorporation of the granule membrane into the plasma membrane. The experimental result that all other inducers did not cause an electrorotation decrease showed that protein-dependent processes before membrane permeabilization were inhibited.

In summary, electrorotation can detect an essential membrane event involving either the permeabilization or an electrical connection of the canicular system to the cell exterior of the plasma membrane in platelets. This information would not be obtained by other means. In this context, electrorotation could be a useful tool in combination with other methods in further studies of platelet release as well as in other cellular systems. The results also showed that the diamide treatment had a complex effect on the platelets. It inhibited very initial step of exocytosis as well as later steps as was demonstrated by the electrorotation decrease still occurring after A 23187 activation, whereas granular release was largely reduced. Measurements on red cells proved that A 23187 at the concentration used alone cannot induce a large enough Ca^{2+} permeability to be detected by electrorotation.

We would like to thank I. Forster from the Department of Physiology, University of Zürich, for critical comments and support in the manuscript preparation, U. Till and P. Spangenberg from the Department of Pathological Biochemistry, Medical Academy of Erfurt for generous support and helpful discussions, and A. M. Ladhoff from the Charité, Berlin for the electron-micrographs.

Part of this work was supported by a grant from Volkswagenstiftung.

REFERENCES

Arnold, W. M., and U. Zimmermann. 1983. Patent application P 3325 843.0, Germany.

Arnold, W. M., and U. Zimmermann. 1988. Electro-rotation: development of a technique for dielectric measurements of individual cells and particles. *J. Electrostatics.* 21:151–191.

Asami, K., and T. Yamaguchi. 1992. Dielectric spectoscopy of plant protoplasts. *Biophys. J.* 63:1493–1499.

Bronner, C., J.-G. Kuhry, and Y. Landry. 1986a. Labelling of the inner side of granules membrane during exocytosis. A method to differentiate secretion processes. *Agents Actions.* 18:53–56.

Bronner, C., Y. Landry, P. Fonteneau, and J.-G. Kuhry. 1986b. A fluorescent hydrophobic probe used for monitoring the kinetics of exocytosis phenomena. *Biochemistry.* 25:2149–2154.

Donath, E., M. Egger, and V. P. Pastushenko. 1990. Dielectric behavior of anion exchange protein of human red blood cells. Theoretical analysis and comparison to electrorotation data. *Bioelectrochem. Bioenerg.* 23: 337–360.

Donath, E., M. Egger, and V. P. Pastushenko. 1993. Electrorotation behavior of aggregated particles. A theoretical study. *Bioelectrochem. Bioenerg.* 31:115–129.

Egger, M., E. Donath, V. P. Pastushenko, and P. Kuzmin. 1991. Electrorotation of dumb-bell shaped particles. Theory and experiment. *Bioelectrochem. Bioenerg.* 26:383–393.

Egger, M., E. Donath, P. Spangenberg, M. Bimmler, R. Glaser, and U. Till. 1988. Human platelet electrorotation change induced by activation: inducer specificity and correlation to serotonin release. *Biochim. Biophys. Acta.* 72:265–276.

Fuhr, G., and P. Kuzmin. 1986. Behavior of cells in rotating electric fields with account to surface charges and cell structures. *Biophys. J.* 50: 789–795.

Fuhr, G., P. Roesch, T. Müller, V. Dressler, and H. Göring. 1990. Dielectric spectroscopy of chloroplasts isolated from higher plants. *Plant Cell Physiol.* 31:975–986.

Gimsa, J., G. Fuhr, and R. Glaser. 1986. Patent application WP O1N/ 281223, Germany.

Gimsa, J., R. Glaser, and G. Fuhr. 1991a. Theory and application of the rotation of biological cells in rotating electric fields (electrorotation). *In* Physical Characterisation of Biological Cells. W. Schütt, H. Klinkmann, I. Lamprecht, and T. Wilson, editors. Verlag Gesundheit, Berlin, Germany. 295–322.

Gimsa, J., P. Marszalek, U. Löwe, and T. Y. Tsong. 1991b. Dielectrophoresis and electrorotation of neurospora slime and murine myeloma cells. *Biophys. J.* 60:5–14.

Gimsa, J., T. Schnelle, G. Zechel, and R. Glaser. 1993. Dielectric spectroscopy of human erythrocytes: investigations under the influence of nystatin. *Biophys. J.* 66:1244–1253.

Heptinstall, S., J. Bevan, S. R. Cockbill, S. P. Hanley, and M. J. Parry. 1980. Effects of a selective inhibitor of thromboxane synthetase on human blood platelet behavior. *Thromb. Res.* 20:219–230.

Hill, T. D., J. G. White, and G. H. Rao. 1989. The influence of gluthatione depleting agents on human platelet function. *Thromb. Res.* 53:457–466.

Hofmann, B., R. Danz, J. Hofmann, J. Pescarmona, A. Bosia, M. Meyer, W. Lösche, and U. Till. 1983. Differences in morphology and protein pattern of human blood platelets during irreversible and diamide mediated reversible aggregation. *Biomed. Biochim. Acta.* 42:489–501.

Kakutani, T., S. Shibatani, and M. Sugai. 1993. Electrorotation of nonspherical cells—theory for ellipsoidal cells with an arbitrary number of shells. *Bioelectrochem. Bioenerg.* 31:131–145.

Kitajima, H., T. Yamaguchi, and E. Kimoto. 1990. Hemolysis of human erythrocytes under hydrostatic pressure is suppressed by cross-linking membrane proteins. *J. Biochem.* 108:1057–1062.

Klonk, S., and B. Deuticke. 1992. Involvement of cytoskeletal proteins in the barrier function of the human erythrocyte membrane. I. Impairment of resealing and formation of aqueous pores in the ghost membrane after modification of SH groups. *Biochim. Biophys. Acta.* 1106:126–136.

Pastushenko, V. P., P. Kuzmin, and Y. A. Chizmadzhev. 1985. Dielectrophoresis and electrorotation: a unified theory for spherically symmetrical cells. *Stud. Biophys.* 110:51–57.

Pastushenko, V. P., P. Kuzmin, and Y. A. Chizmadzhev. 1988. Dielectrophoresis and electrorotation of cells: unified theory for spherically symmetric cells with arbitrary structure of membrane. *Biol. Membr.* 5:65–78.

Sauer, S. A., and W. Schlögel. 1985. Torques exerted on cylinders and spheres by external electromagnetic fields. A contribution to the theory of field induced cell rotation. *In* Interactions between Electromagetic Fields and Cells. A. Chiabrera, C. Nicolini, and H.-P. Schwan, editors. Plenum Press, New York. 1–49.

Spangenberg, P., U. Till, S. Gschmeissner, and N. Crowford. 1987. Changes in the distribution and organization of platelet actin induced by diamide and its functional consequences. *Br. J. Haematol.* 67:443–450.

Wang, X.-B., Y. Huang, R. Hölzel, P. H. Burt, and R. Pethig. 1993. Theoretical and experimental investigations of the interdependence of the dielectric, dielectrophoretic and electrorotational behaviour of colloidal particles. *J. Phys. D Appl. Phys.* 26:312–322.

Wu, X.-B., B. Brune, F. von Appen, and V. Ullrich. 1992. Reversible activation of soluble guanylate cyclase by oxidizing agents. *Arch. Biochem. Biophys.* 294:75–82.